

Article

Fabrication of Noble-Metal-Free Mo₂C/CdIn₂S₄ Heterojunction Composites with Elevated Carrier Separation for Photocatalytic Hydrogen Production

Hong Qiu, Xiaohui Ma, Hongxia Fan, Yueyan Fan, Yajie Li, Hualei Zhou * and Wenjun Li *

Beijing Key Laboratory for Science and Application of Functional Molecular and Crystalline Materials, University of Science and Technology Beijing, Beijing 100083, China

* Correspondence: hlzhou@ustb.edu.cn (H.Z.); wjli_ustb@163.com (W.L.)

Abstract: Molybdenum-based cocatalyst being used to construct heterojunctions for efficient photocatalytic H₂ production is a promising research hotspot. In this work, CdIn₂S₄ was successfully closely supported on bulk Mo₂C via the hydrothermal method. Based on their matching band structures, they formed a Type I heterojunction after the combination of Mo₂C (1.1 eV, −0.27 V, 0.83 V) and CdIn₂S₄ (2.3 eV, −0.74 V, 1.56 V). A series of characterizations proved that the heterojunction composite had higher charge separation efficiency compared to a single compound. Meanwhile, Mo₂C in heterojunction could act as an active site for hydrogen production. The photocatalytic H₂ production activity of the heterojunction composites was significantly improved, and the maximum activity was up to 1178.32 μmol h^{−1} g^{−1} for 5Mo₂C/CdIn₂S₄ composites. 5Mo₂C/CdIn₂S₄ heterojunction composites possess excellent durability in three cycles (loss of 6%). Additionally, the mechanism of increased activity for composites was also investigated. This study provides a guide to designing noble-metal-free photocatalyst for highly efficient photocatalytic H₂ evolution.

Keywords: noble-metal-free; Mo₂C; CdIn₂S₄; heterojunction; carrier separation



Citation: Qiu, H.; Ma, X.; Fan, H.; Fan, Y.; Li, Y.; Zhou, H.; Li, W. Fabrication of Noble-Metal-Free Mo₂C/CdIn₂S₄ Heterojunction Composites with Elevated Carrier Separation for Photocatalytic Hydrogen Production. *Molecules* **2023**, *28*, 2508. <https://doi.org/10.3390/molecules28062508>

Academic Editor: Yucheng Lan

Received: 19 January 2023

Revised: 7 March 2023

Accepted: 7 March 2023

Published: 9 March 2023



Copyright: © 2023 by the authors. Licensee MDPI, Basel, Switzerland. This article is an open access article distributed under the terms and conditions of the Creative Commons Attribution (CC BY) license (<https://creativecommons.org/licenses/by/4.0/>).

1. Introduction

With the increasingly serious energy crisis, H₂ energy is attracting more and more attention due to its renewable, clean, high energy density, and so on [1–3]. As a feasible method, photocatalytic H₂ production from water has been a research hotspot among all the methods of H₂ production [4–6]. Proverbially, developing stable and high-efficiency visible light photocatalyst is always a core challenge for photocatalysis technology [7,8]. To date, numerous semiconductors—including sulfides, metal oxides, and nitrides—have been extensively exploited for photocatalytic H₂ production [9–11]. Among the developed photocatalysts, CdIn₂S₄ (CIS) is of great interest [12–14]. Nevertheless, for bare CIS, the low carrier separation efficiency and lack of active site still need to be urgently solved. To address those issues, various methods have been carried out to obtain elevated photocatalytic activity of CdIn₂S₄-based photocatalysts, such as tuning the morphologies [15], constructing heterojunctions [16,17], doping metal or nonmetal elements [18,19], and so on. He et al. [20] prepared ultra-thin CdIn₂S₄ nanosheets to acquire efficient photocatalytic activity. Chen et al. [21] designed CdIn₂S₄/TiO₂ Z-scheme heterojunction with high carrier separation efficiency for photocatalytic H₂ production. Yu et al. [17] reported that PdS-loaded ZnIn₂S₄/CdIn₂S₄ flower-like microspheres had significantly improved photocatalytic activity and high-efficiency stability under aqueous Na₂SO₃ and Na₂S solution. Guo et al. [12] prepared CdIn₂S₄/CNFs/Co₄S₃ nanofiber networks with efficient charge separation and adequate active sites for H₂ production using solar-driven water splitting. Additionally, cocatalysts are critical for booting carrier separation efficiency and causing the active site of H₂ production to increase the activity of photocatalysts. Proverbially,

noble metals (e.g., Pt, Au) have been proven to be the most effective cocatalysts for photocatalytic H₂ production [22]. Regrettably, the scarcity of noble metals greatly restricts their extensive utilization. Accordingly, exploiting accessible and low-priced cocatalysts is of great significance for achieving high-efficiency photocatalytic H₂ production.

As a type of transition metal carbide, Mo₂C has been widely studied in the field of electrocatalysis due to its good electric conductivities and high catalytic properties [23,24]. Universally, electrocatalysts with superior activity can also be used as efficient cocatalysts for photocatalytic hydrogen production. Therefore, Mo₂C has great potential for photocatalytic H₂ evolution [25–27]. In our previous study, our group prepared In₂S₃@Mo₂C heterojunction for photocatalytic H₂ generation, revealing that Mo₂C was a highly H₂-generation-active cocatalyst [27]. Yue et al. [28] designed a SrTiO₃@Mo₂C core-shell nanostructure with enhanced charge separation for dramatically elevated photocatalytic H₂ evolution. Yue et al. [29] prepared dandelion-like Mo₂C/TiO₂ heterojunction photocatalysts with efficient charge separation and catalytically active sites for photocatalytic H₂ evolution. Zhang et al. [30] reported g-C₃N₄/Mo₂C hybrid photocatalysts in which, as a cocatalyst, Mo₂C on the surface of g-C₃N₄ leads to promoted charge separation, improved visible light absorption, and enhanced following H₂-evolution rate. In this sense, after Mo₂C is combined with matched CdIn₂S₄, it may be an ideal heterojunction system for enhanced photocatalytic H₂ generation. In heterojunction, Mo₂C could not only accelerate the separation efficiency of photogenerated carriers but could also act as an active site of H₂ production. Moreover, it is worth noting that the Mo₂C/CdIn₂S₄ system has not been reported for photocatalytic performance.

In this work, we successfully synthesized a novel non-noble-metal Mo₂C/CdIn₂S₄ heterostructure for photocatalytic H₂ production in which CdIn₂S₄ nanoparticles were loaded on bulk Mo₂C. Under solar light irradiation, in heterojunction, Mo₂C could trap photo-generated electrons of CdIn₂S₄ to efficiently accelerate carrier separation. Meanwhile, the electrons could reduce water to hydrogen at the active site of Mo₂C. As a result, the Mo₂C/CdIn₂S₄ composites displayed visibly elevated H₂ production activity up to 1178.32 μmol h⁻¹ g⁻¹. Highly significantly, the designed heterojunction composites possessed outstanding stability, and the mechanism of photocatalytic activity enhancement was investigated. This work offers a thinking to design non-noble-metal heterostructure with high carriers separation efficiency for photocatalytic H₂ production.

2. Results and Discussion

The morphologies of all samples were obtained via scanning electron microscopy (SEM), transmission electron microscopy (TEM), and high-resolution transmission electron microscopy (HRTEM). Figure 1A showed that CdIn₂S₄ had nanoparticle structures with sizes of 25–180 nm, and Figure 1B displayed that Mo₂C had a bulk structure about 1–2 μm in size. Figure 2A,B also showed that CdIn₂S₄ and Mo₂C had nanoparticle structures and bulk structures, which confirmed the results of scanning electron microscopy. Figure 1C clearly revealed that CdIn₂S₄ was deposited on the surface of Mo₂C. Simultaneously, compared to the pure molybdenum carbide, Figure 2C shows that the massive molybdenum carbide edge had many CdIn₂S₄ particles, which also confirmed the results of the scanning electron microscopy. The results of high-resolution transmission electron microscopy were analyzed to further confirm the formation of MS heterojunction composites. Figure 2D,E represented that the lattice fringe spacings of (3 1 1) planes (CdIn₂S₄) and (1 0 1) planes (Mo₂C) were 0.33 nm and 0.21 nm, respectively. More significantly, Figure 2F possessed two lattice fringes of 0.33 nm and 0.21 nm assigned to the (3 1 1) planes of CdIn₂S₄ [31] and the (1 0 1) planes of Mo₂C [27], respectively, which demonstrated the simultaneous presence of CdIn₂S₄ and Mo₂C in the MS heterojunction composites. In a word, the aforementioned results corroborated the successful synthesis of the heterojunction composites.

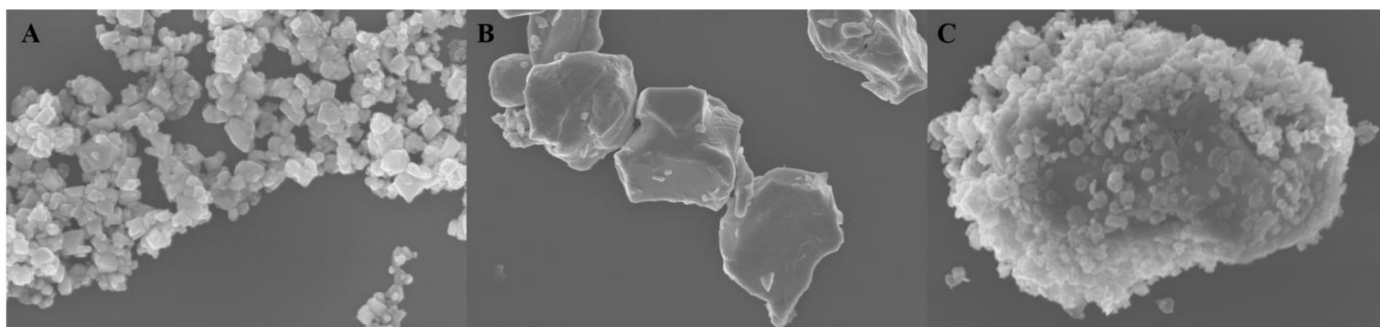


Figure 1. The scanning electron microscopy (SEM) of CdIn₂S₄ (A), Mo₂C (B), and 5MS (C) heterojunction composites.

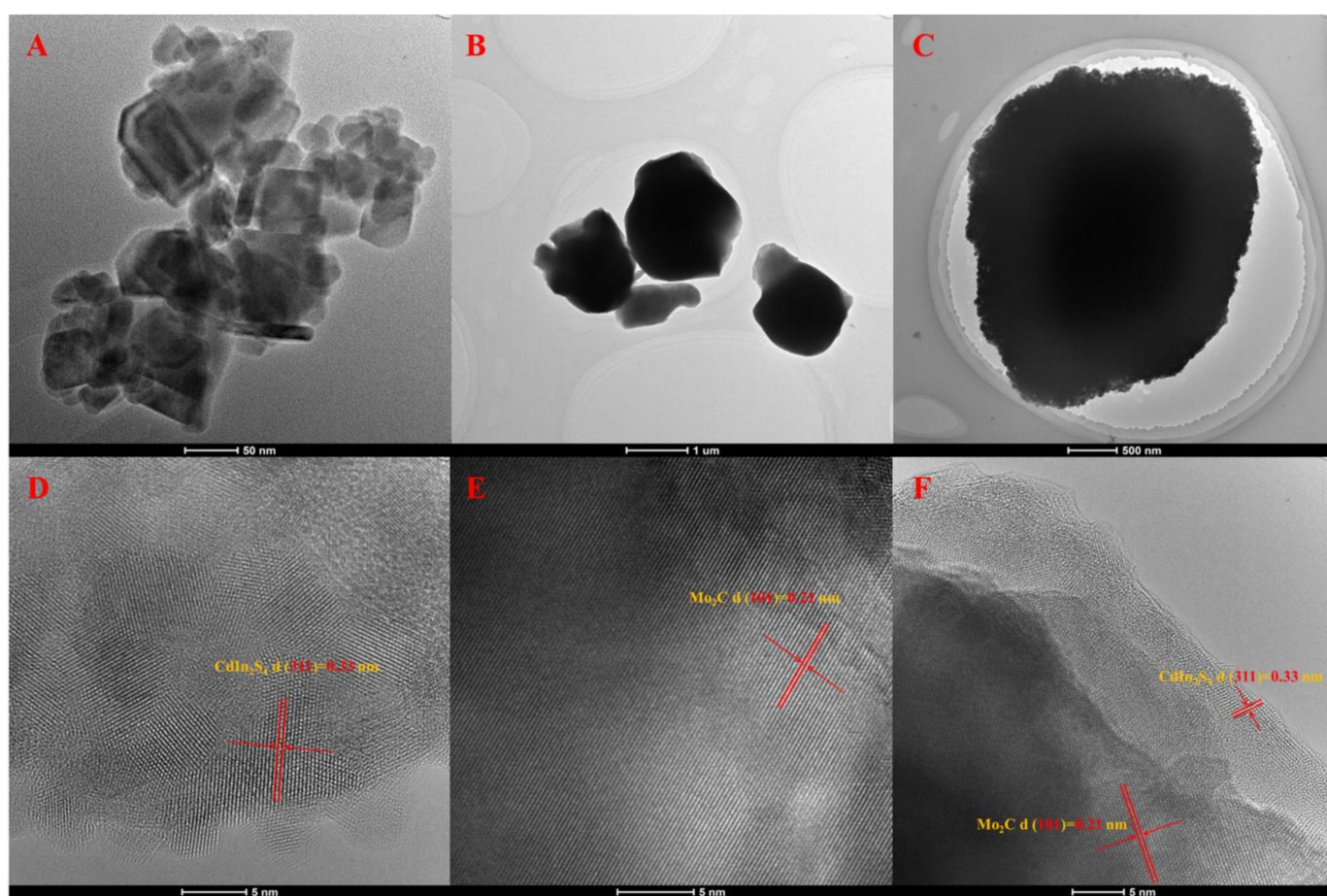


Figure 2. The transmission electron microscopy (TEM) and high-resolution transmission electron microscopy (HRTEM) of CdIn₂S₄ (A,D), Mo₂C (B,E), and 5MS (C,F) heterojunction composites.

In Figure 3, the optical properties of CdIn₂S₄, Mo₂C, and the 5MS hybrid were discreetly studied via UV–Vis diffuse reflectance spectra. As expected, CdIn₂S₄ possessed an evident edge at about 575 nm that was derived from its transition of the band [15]. Bare Mo₂C was black and revealed a broad and strong visible light absorption capacity from 300 nm to 800 nm. Interestingly, it was found that the absorption edge of heterojunction composites extended to longer wavelength regions compared to bare CdIn₂S₄. Meanwhile, the visible light absorption intensity of heterojunction composites was visibly boosted at 500–800 nm with increasing Mo₂C content. The stronger visible light absorption capacity plays a pivotal role in achieving solar energy conversion. Based on our previous research [27], the band gaps (E_g) of Mo₂C and CdIn₂S₄ were 1.1 eV and 2.3 eV, respectively,

which conform to the literature values well [29,31]. It can be clearly seen that the band gap of MS heterojunction composites is reduced compared to CdIn₂S₄ in Figure S1. As shown in Figure 3B, at a frequency of 1 kHz, Mott–Schottky (M-S) tests were carried out to analyze the type of semiconductors and the charge transfer process. The straight lines of Mo₂C and CdIn₂S₄ both have positive slopes, which suggests that they are intrinsic n-type characteristics. Additionally, the conduction band potential values are confirmed on the basis of extrapolation of the straight line toward the x-axis. As everyone knows, the flat band potential is around equal to the conduction band potential for semiconductors with intrinsic n-type characteristics. In line with the intercept of the M-S plots (Figure 3B,C), the conduction band potentials (E_{CB}) of Mo₂C and CdIn₂S₄ are and -0.27 V and -0.74 V, respectively. Obviously, the conduction band potential of Mo₂C is more positive than the conduction band potential of CdIn₂S₄, and this difference in energy level will help drive electron transfer from the conduction band potential of CdIn₂S₄ to the conduction band potential of Mo₂C for photocatalytic hydrogen production. Therefore, on the basis of the following formula, the valence bands (E_{VB}) of Mo₂C and CdIn₂S₄ are 0.83 V and 1.56 V, respectively.

$$E_{VB} = E_{CB} + E_g \quad (1)$$

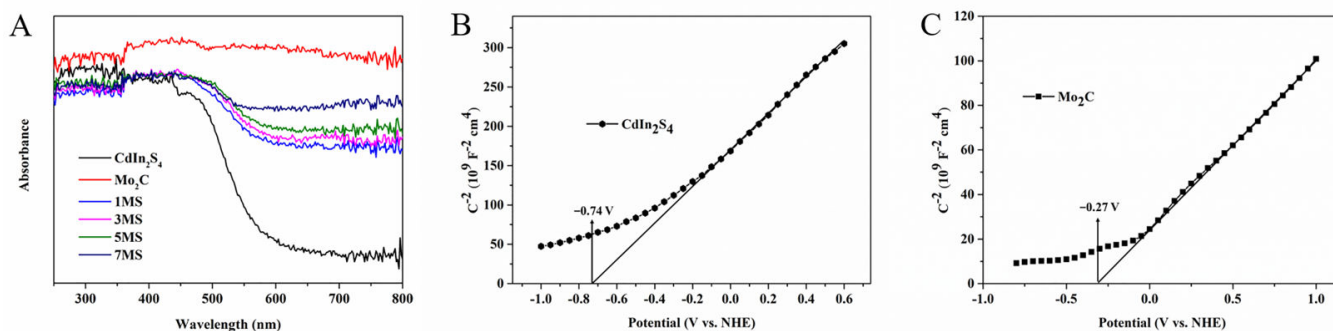


Figure 3. The UV–Vis diffuse reflectance spectra of CdIn₂S₄, Mo₂C, and MS heterojunction composites (A); Mott–Schottky plots for CdIn₂S₄ (B) and Mo₂C (C).

The phase of prepared samples is authenticated and discussed via X-ray diffraction patterns (XRD), and the results are illustrated in Figure 4. All as-prepared samples possessed sharp diffraction peaks, indicating excellent crystallinity. The patterns of CdIn₂S₄ and Mo₂C were confirmed to be cubic (JCPDF: 27-0060) and hexagonal (JCPDF: 35-0787) structures, respectively [26,32]. The peaks around 2θ of 14.2° , 23.1° , 27.3° , 33.1° , 43.3° , and 47.4° were readily instructed to those of CdIn₂S₄ and accorded to the (1 1 1), (2 2 0), (3 1 1), (4 0 0), (4 4 0), and (6 2 2) planes, respectively [32]. For bare Mo₂C, the peaks at 34.4° , 38.0° , 39.4° , 52.2° , 61.5° , and 69.5° were observed and assigned to the (1 0 0), (1 0 1), (1 1 0), (0 0 2), (2 0 0), and (2 0 1) planes, respectively [26]. The heterojunction composites still held the evident characteristic peaks of CdIn₂S₄ ((2 2 0), (3 1 1), (4 0 0), (4 4 0), and (6 2 2) planes) after the hybridization of CdIn₂S₄ and Mo₂C. Although the peaks of Mo₂C have low contents, the (1 0 0), (1 0 1), (1 1 0), and (0 0 2) planes of Mo₂C could be observed at 34.4° , 38.0° , 39.4° , and 52.2° , respectively in heterojunction composites [27]. The peak intensity of Mo₂C significantly increased along with the elevation of the Mo₂C content, which was advantageous for photocatalytic hydrogen production and had been studied in previous reports. The X-ray diffraction patterns (XRD) results demonstrated that MS composites were successfully fabricated, which is consistent with scanning electron microscopy (SEM), transmission electron microscopy (TEM), and high-resolution transmission electron microscopy (HRTEM) results.

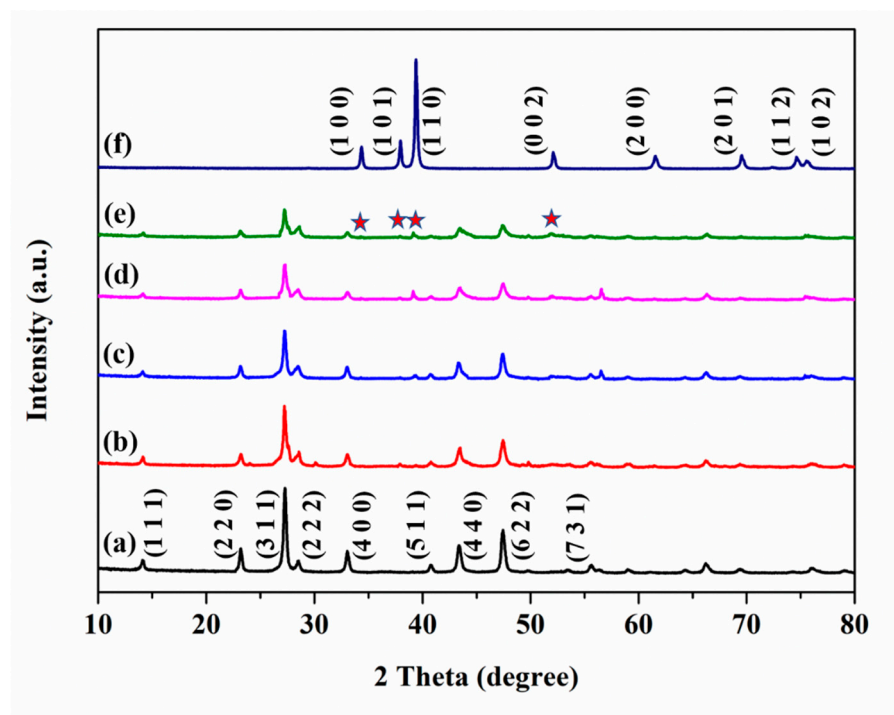


Figure 4. The X-ray diffraction patterns, of CdIn₂S₄, Mo₂C, and MS heterojunction composites ((a) CdIn₂S₄; (b) 1MS; (c) 3MS; (d) 5MS; (e) 7MS; (f) Mo₂C). ★ is peaks of Mo₂C, the (1 1 1), (2 2 0), (3 1 1), (4 0 0), (5 1 1), (4 4 0), (6 2 2), and (7 3 1) planes corresponds to CdIn₂S₄, the (1 0 0), (1 0 1), (1 1 0), (0 0 2), (2 0 0), (2 0 1), (1 1 2), and (1 0 2) planes corresponds to Mo₂C).

Subsequently, we also utilized X-ray photoelectron spectroscopy (XPS) to further analyze and study the composition of the photocatalysts as well as the strong electronic interactions between CdIn₂S₄ and Mo₂C. Figure 5A displays the full XPS survey of 5MS composites, and the full XPS survey explains the existence of Mo, Cd, C, S, and In elements in the ternary composites, which shows that the heterojunction composites are prepared successfully. In Figure 5B, for bare CdIn₂S₄, the peaks at 412.2 eV and 405.5 eV correspond to Cd 3d_{3/2} and Cd 3d_{5/2}, respectively, and In 3d_{3/2} and In 3d_{5/2}, respectively, which are the characteristic peaks of Cd²⁺ and In³⁺ in CdIn₂S₄. In Figure 5C, for bare CdIn₂S₄, the peaks at 452.5 eV and 444.9 eV correspond to In 3d_{3/2} and In 3d_{5/2}, respectively, which are the characteristic peaks of In³⁺ in CdIn₂S₄. In Figure 5B, for 5MS composites, the peaks at 412.1 eV and 405.3 eV correspond to Cd 3d_{3/2} and Cd 3d_{5/2}, respectively, which are the characteristic peaks of Cd²⁺ in the ternary composites. In Figure 5C, for 5MS composites, the peaks at 452.3 eV and 444.8 eV correspond to In 3d_{3/2} and In 3d_{5/2}, respectively, which are the characteristic peaks of In³⁺ in the ternary composites. In Figure 5D, the S 2p data of CdIn₂S₄ centered at binding energies of 162.9 eV and 161.7 eV match with S 2p_{1/2} and S 2p_{3/2}, respectively. In Figure 5D, the S 2p data of 5MS heterojunction composites centered at binding energies of 162.8 eV and 161.6 eV match with S 2p_{1/2} and S 2p_{3/2}, respectively. Nevertheless, a distinct peak at about 169.0 eV could be seen, distributing SO₄²⁻ resulting from hydrothermal processes in Figure 5D. For Mo 3d spectra of bare Mo₂C (Figure 5E), there were three peaks of Mo 3d in Mo₂C situate at 233.0 eV, 228.7 eV, and 236.1 eV, corresponding to Mo 3d_{3/2}, Mo 3d_{5/2}, and Mo-O band, respectively. It can also be seen that Mo mainly exists in three forms (Mo 3d_{5/2} and 227.7 eV, Mo 3d_{3/2} and 232.5 eV, Mo-O and 235.7 eV) in 5MS composites in Figure 5E. Furthermore, in Figure 5E, there is a distinct peak of 225.9 eV in 5MS composites, which can be attributed to S 2s, which is also consistent with our previous research and what others have reported. In Figure 5F, for C 1s spectra of Mo₂C, in addition to the carbon standard peak (284.8 eV), there are two peaks located at 286.4 eV and 288.9 eV, assigned to C-O and C=O, respectively. The binding

energies of C-O and C=O in 5MS composites are 286.8 eV and 288.9 eV, respectively, in Figure 5F. After the hybridization of CdIn₂S₄ and Mo₂C, the binding energies of all elements have shifted slightly compared to pure CdIn₂S₄ and Mo₂C, indicating a strong interaction between CdIn₂S₄ and Mo₂C, which is very advantageous for photocatalytic hydrogen production [33,34]. The X-ray photoelectron spectroscopy (XPS) results support the X-ray diffraction patterns (XRD), scanning electron microscopy (SEM), transmission electron microscopy (TEM), and high-resolution transmission electron microscopy (HRTEM) results.

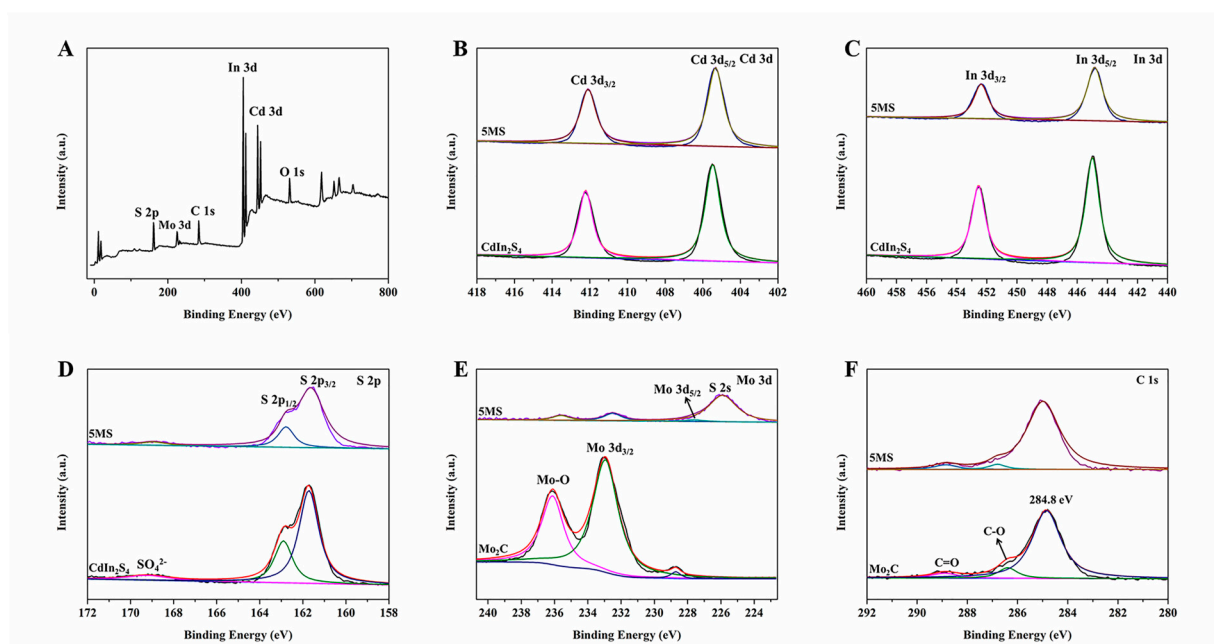


Figure 5. The X-ray photoelectron spectroscopy of CdIn₂S₄, Mo₂C, and MS heterojunction composites ((A): full survey; (B): Cd 3d; (C): In 3d; (D): S 2p; (E): Mo 3d; (F): C 1s).

The photocatalytic behavior of all samples was assessed via photocatalytic experiment under visible light irradiation ($\lambda \geq 420$ nm) (Figure 6). CdIn₂S₄ revealed low photocatalytic activity due to the scarce active site and rapid carrier recombination. Additionally, for Mo₂C, there was no photocatalytic activity because of the rapid carrier recombination resulting from a narrow band gap, coinciding well with the results reported [35]. Extraordinarily, after CdIn₂S₄ was incorporated with Mo₂C, the photocatalytic activities of MS composites increased sharply. The above H₂ production process also confirms the results of photocatalysis and electrochemistry, that is, after the combination of Mo₂C and CdIn₂S₄, not only was the photogenerated carrier separation efficiency improved, but the H₂ production activity was surprisingly increased as well. In Figure 6A, the amount of H₂ produced was severally 973.4 $\mu\text{mol/g}$ (1MS), 3681.5 $\mu\text{mol/g}$ (3MS), 6313.6 $\mu\text{mol/g}$ (5MS), and 4596.9 (7MS) $\mu\text{mol/g}$ in 5 h. In Figure 6B, the corresponding average H₂ production rate of MS composites was 181.67 $\mu\text{mol h}^{-1} \text{g}^{-1}$, 687.08 $\mu\text{mol h}^{-1} \text{g}^{-1}$, 1178.32 $\mu\text{mol h}^{-1} \text{g}^{-1}$, and 857.94 $\mu\text{mol h}^{-1} \text{g}^{-1}$, respectively. Notably, when the content of Mo₂C increased, the H₂ production rates displayed a volcano-shaped photoactivity trend. The best weight ratio of Mo₂C was determined to be 5 wt%, and the photocatalytic activity could reach the maximum value. This obvious improvement might stem from (i) Mo₂C acting as active sites for water reduction; (ii) the separation efficiency of MS heterojunction structures being distinctly boosted. However, after the content of Mo₂C exceeds 5%, the photocatalytic activity gradually reduced. This is because high Mo₂C can not only block visible light absorption of CdIn₂S₄ but can also serve as the recombination center of carriers, resulting in the suppression of electron–holes separation [30,36]. The above results imply the appropriate Mo₂C is significant for optimizing the photocatalytic activity of photocatalyst. Moreover, as shown in Figure 6B, the stability tests of photocatalytic hydrogen production

for 5MS composites are also determined. There was a slight drop in hydrogen production per cycle, probably due to the loss of the photocatalyst during filtration and washing. Significantly, in three photocatalytic tests, 5MS composites reveal highly stable photocatalytic performance (Figure 6C). The comparison of photocatalytic performance between this work and the current work with similar work was in Supplementary Materials Table S2.

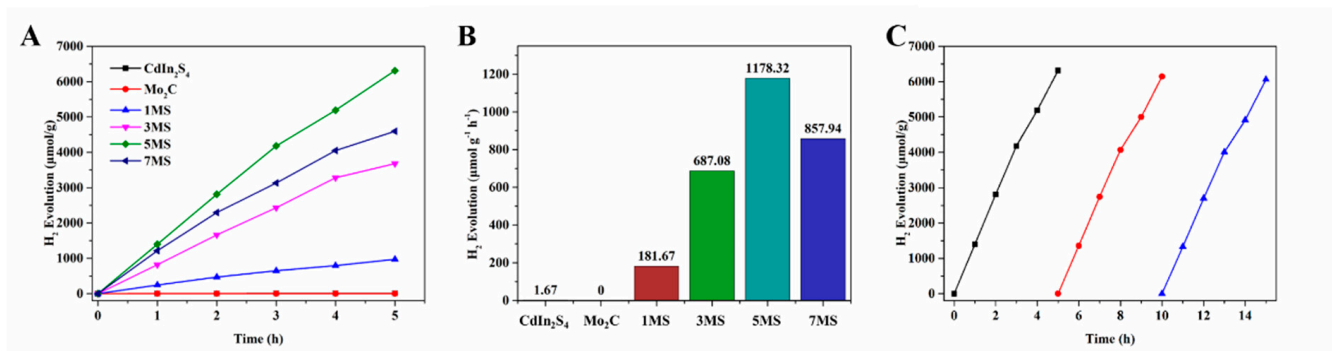


Figure 6. The amount of hydrogen produced over time (A); average rate of hydrogen production (B); stability of 5MS samples (C). Black is the first cycle, red is the second cycle, and blue is the third cycle.

To explore the carrier separation of photocatalysts, the PL and a series of electrochemical tests are obtained and studied (Figure 7). Generally, photoluminescence (PL) spectroscopy is one of the commonly used methods for evaluating the efficiency of photo-generated electron–hole pair charge separation. Due to its intrinsic properties, different photocatalysts have different emission spectra. For photocatalysts, the lower PL emission peak intensity means the lower recombination of photogenerated charge [37]. Figure 7A display that MS composites possess lower peak than bare CdIn_2S_4 , which means that composites have higher carrier separating efficiency after the CdIn_2S_4 is supported on the surface of Mo_2C cocatalyst. Therefore, the addition of Mo_2C can increase the carrier separation of the catalyst. Figure 7B reveals the transient photocurrent responses (TPR) of all photocatalysts to investigate the charge transfer under simulated solar irradiation. Under visible light, the photocurrent responses of all photocatalysts were improved. As expected, it can be seen that all MS composites have stronger photocurrent than CdIn_2S_4 , effectively implying charge transfer for composites [38]. The order of photocurrent intensity is: $\text{CdIn}_2\text{S}_4 < 1\text{MS} < 3\text{MS} < 7\text{MS} < 5\text{MS}$. The orders are in keeping with the photocatalytic H_2 production results. The higher photocurrent indicates faster and more efficient e^- migration from CB of CdIn_2S_4 to CB of Mo_2C , followed by a reduction reaction. In addition, the photocurrent result is in good agreement with results of PL above and EIS below. The electrochemical impedance spectroscopy (EIS) was measured and recorded on the open circuit potential under visible light. The EIS Nyquist plot is also used to understand the charge transfer of photocatalysts [39]. As shown in Figure 7C, compared to pure CdIn_2S_4 , the semicircle curves of EIS for the MS heterojunction composites are shown, which indicates that photoinduced carriers are tardy recombination and affect migration with the addition of Mo_2C . The order of radius is: $5\text{MS} < 7\text{MS} < 3\text{MS} < 1\text{MS} < \text{CdIn}_2\text{S}_4$, matching with the photocurrent results. The illustration in Figure 7C is a model circuit. Moreover, 5MS composites have the smallest arcs compared to other samples. This result implied 5MS composites' presence faster than electron migration and interface electron migration resistance. In summary, the PL and electrochemical results of all samples illustrate that Mo_2C could speed up charge separation efficiency to obtain many more free electrons for photocatalytic hydrogen production.

Based on band arrangement and characterization results, the probable photocatalytic mechanism of heterojunction composites is designed and explained to verify the elementary reason for the distinct amendment of the photocatalytic performance of the MS heterojunction photocatalyst (Figure 8). The low H_2 activity of CdIn_2S_4 may be due to the scarce active

site and rapid carrier recombination. In the MS heterojunction, Mo₂C is an electron capture trap, which can quickly extract photoinduced electrons generated in CdIn₂S₄, accelerate the separation of photoinduced electron–hole pairs and reach higher photocatalytic hydrogen production. Clearly, a Type I heterojunction could be formed because the conduction band of Mo₂C is more positive than that of CdIn₂S₄ and the valence band of Mo₂C is more negative than that of CdIn₂S₄. The electron of the valence band for Mo₂C and CdIn₂S₄ could be stimulated to the conduction band by visible light. Due to excellent electrical conductivity, Mo₂C can rapidly capture the electrons of CdIn₂S₄ before the charge recombination, so it appears that the electrons of conduction band for CdIn₂S₄ transferred to the conduction band of Mo₂C. Electrons on Mo₂C could reduce water to hydrogen ($H^+ + e^- \rightarrow 0.5H_2$). In the public eye, the separation and recombination of charge carrier are two competitive processes. Considering the different transfer rates of e^- and h^+ from CdIn₂S₄ to Mo₂C and the excellent metallic conductivity of Mo₂C, the h^+ in the VB of CdIn₂S₄ partially transfers to the valence band of Mo₂C, and the remaining h^+ in the valence band of CdIn₂S₄ and the h^+ in the valence band of Mo₂C reacts with lactic acid, thereby reducing the surface charge recombination. The formation of a Type I heterojunction greatly improves the separation rate of carriers, demonstrated clearly by PL and electrochemical results. This obvious improvement might stem from (i) Mo₂C acting as active sites for water reduction and (ii) the separation efficiency of MS heterojunction structures being distinctly boosted. Based on these results, synergetic modification of carrier separation and active sites result in the remarkably elevated photocatalytic activity of MS heterojunction composites.

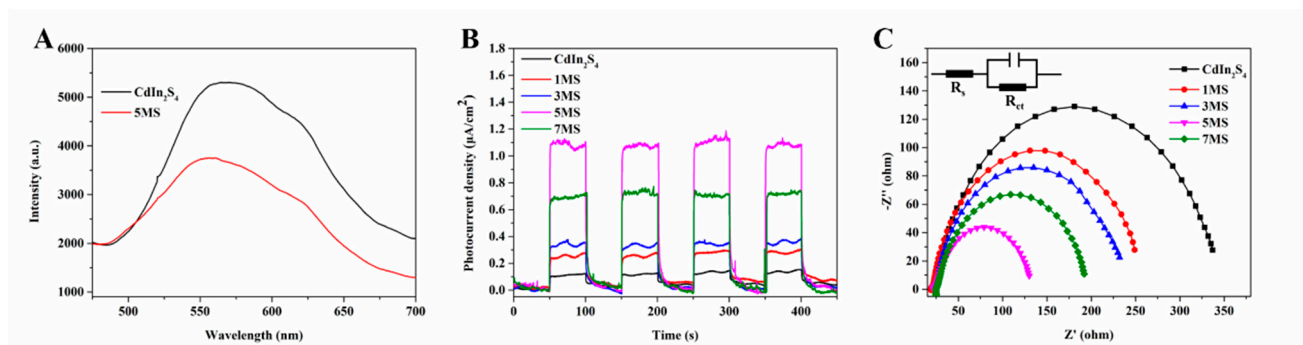


Figure 7. PL at an excitation wavelength of 469 nm (A); TPR (B) and EIS (C) for as-prepared samples.

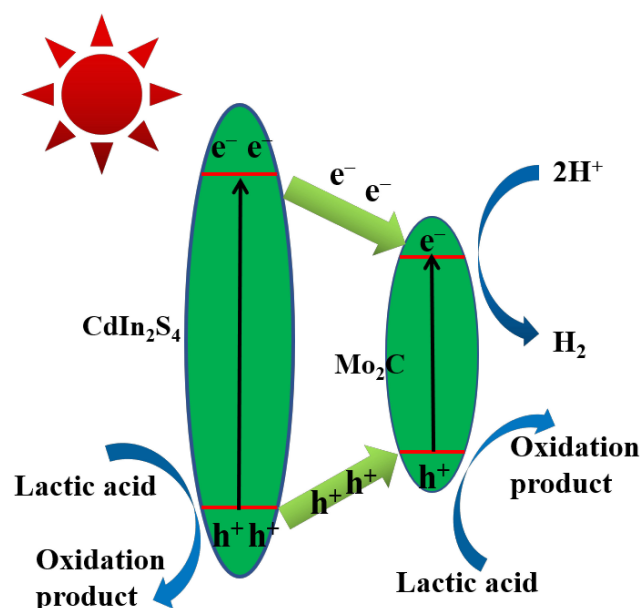


Figure 8. The photocatalytic hydrogen schematic diagram of MS heterojunction composites.

3. Experiment

3.1. Reagents

Molybdenum carbide (Mo_2C , 325 mesh, $\geq 99.5\%$) was acquired from Saen Chemistry Technology (Shanghai, China). Indium(III) nitrate hydrate ($\text{In}(\text{NO}_3)_3 \cdot 3\text{H}_2\text{O}$), thioacetamide (TAA), cadmium nitrate ($\text{Cd}(\text{NO}_3)_2 \cdot 4\text{H}_2\text{O}$), and lactic acid were all obtained from Aladdin.

3.2. Synthesis of CdIn_2S_4 and $\text{Mo}_2\text{C}-\text{CdIn}_2\text{S}_4$

Synthesis of CdIn_2S_4 . Amounts of 2 mmol $\text{In}(\text{NO}_3)_3 \cdot 3\text{H}_2\text{O}$, 4 mmol thioacetamide, and 1 mmol $\text{Cd}(\text{NO}_3)_2 \cdot 4\text{H}_2\text{O}$ were sequentially added to 70 mL deionized water. After stirring for 1 h, turbid liquids were transferred to a Teflon-lined steel autoclave. The resulting reaction was heated at 180 °C for 24 h. After cooling to room temperature, the products were collected via centrifugation, washed with deionized water and ethanol several times, and then dried at 60 °C for 12 h.

Synthesis of $\text{Mo}_2\text{C}-\text{CdIn}_2\text{S}_4$. Amounts of 2 mmol $\text{In}(\text{NO}_3)_3 \cdot 3\text{H}_2\text{O}$, 0.1175 g Mo_2C , 4 mmol thioacetamide, and 1 mmol $\text{Cd}(\text{NO}_3)_2 \cdot 4\text{H}_2\text{O}$ were sequentially added in 70 mL deionized water. Then, the turbid liquids were kept at 180 °C for 24 h. After cooling to room temperature, the products were collected via centrifugation, washed with deionized water and ethanol several times, and then dried at 60 °C for 12 h. The heterojunction composites containing 0.2 g of CdIn_2S_4 with 0.01 g of Mo_2C were labeled as 5MS photocatalysts. The other $\text{Mo}_2\text{C}/\text{CdIn}_2\text{S}_4$ photocatalysts were prepared by introducing different amounts of Mo_2C into the solution with other reaction parameters fixed. Similarly, the samples of CdIn_2S_4 with 1, 3, and 7 mass percent Mo_2C are labeled as 1MS, 3MS, and 7MS, respectively. The additional experiments for optimization of the amounts and conditions were not used in the synthesis process.

3.3. Characterization

The crystal structures of pristine Mo_2C , CdIn_2S_4 , and $\text{Mo}_2\text{C}/\text{CdIn}_2\text{S}_4$ were tested using Cu K α radiation ($\lambda = 1.5406 \text{ \AA}$, 40 kV and 40 mA) in X-ray diffraction patterns (XRD, D/Max-RB, Rigaku, Japan). Transmission electron microscopy (TEM), high-resolution transmission electron microscopy (HRTEM) (F-20, FEI, Hillsboro, OR, USA), and scanning electron microscopy (SEM) (S-4800; Hitachi, Tokyo, Japan) images were obtained. UV–Vis diffuse reflectance spectra (DRS) were carried out using a T9S spectrophotometer with BaSO_4 as a reflectance standard. X-ray photoelectron spectroscopy (XPS) analysis was examined with a monochromatic X-ray source manufactured on an X-ray photoelectron spectrometer (Thermo Fisher Scientific K-Alpha, Waltham, MA, USA). The photoluminescence (PL) was observed using a fluorescence spectrophotometer (F-4500, Hitachi, Tokyo, Japan) with a Xe lamp as the excitation light source.

3.4. Electrochemical Measurements

The electrochemical impedance spectroscopy (EIS)–photocurrent measurement (TPR) curves of photocatalysts were obtained using a CHI660E electrochemical workstation. The samples, a saturated calomel electrode (SCE), and a Pt wire were employed as the working electrode, reference electrode, and counter electrode, respectively. All electrochemical tests used incandescent lamps under visible light. The aqueous solution of Na_2SO_4 (0.5 mol L^{-1}) served as the electrolyte. In total, 5 mg of photocatalyst was suspended in mixed solution with ethanol and Nafion. The as-prepared samples were dispersed into a circle with a diameter of 6 mm on the bottom-middle of an ITO glass matrix using a micropipette and dried at room temperature.

3.5. Photocatalytic H_2 Evolution Test

The photocatalytic H_2 evolution reaction was operated in a typical reaction system according to our previous reports [40–42]. The photocatalytic experiment was carried out under visible light ($\lambda \geq 420 \text{ nm}$). The information of used Xenon lamp and the intensity of

the incident radiation entering the photoreactor were added in Supplementary Materials. First, 30 mL of lactic acid/H₂O solution (10% (v/v) pH = 2.2) was prepared, then 30 mg samples were added in the above solution by ultrasound treatment for 30 min. Before irradiation, the air in reaction container was driven out through the high-purity argon (Ar) gas for 0.5 h. The amount of hydrogen generation was tested via gas chromatography (GC-7920, TCD). Furthermore, stability tests were also carried out to evaluate the stability of MS photocatalysts in three continuous experiments. For the next test, the samples were collected via centrifugation and washing thoroughly with ethanol and water several times and were then dried at 60 °C after every test for H₂ generation.

4. Conclusions

In this research, the novel noble-metal-free Mo₂C/CdIn₂S₄ composites were firstly developed via a facile fabrication process for highly efficient photocatalytic H₂ production. The structure, morphology, and performance of heterojunction composites were analyzed using different characterization techniques. The visible light photocatalytic properties of the Mo₂C/CdIn₂S₄ composites were investigated, and the best photocatalytic activity was up to 1178.32 μmol h⁻¹ g⁻¹ for 5Mo₂C/CdIn₂S₄ composites. Notably, the heterojunction composites possessed high stability in three cycles. The remarkable elevated photocatalytic activity may be due to the accelerated separation efficiency and more active sites for photocatalytic water splitting. We believe that Mo₂C, as noble-metal-free cocatalyst to modify other photocatalysts, has great potential for efficient photocatalytic hydrogen production.

Supplementary Materials: The following supporting information can be downloaded at: <https://www.mdpi.com/article/10.3390/molecules28062508/s1>, Figure S1: Tacu's curve of MS heterojunction composites; Table S1: The incident radiation intensity entering the photoreactor is shown in the table below; Table S2: Comparison of hydrogen evolution data of Mo₂C/CdIn₂S₄ composites compared with other literature reports.

Author Contributions: Conceptualization, H.Q. and X.M.; Methodology, H.Q.; Formal analysis, X.M. and Y.F.; Investigation, H.Q.; Resources, H.Z.; Data curation, X.M. and Y.L.; Writing—original draft, H.Q.; Writing—review & editing, H.Q.; Supervision, H.F.; Project administration, W.L.; Funding acquisition, W.L. All authors have read and agreed to the published version of the manuscript.

Funding: The National Natural Science Foundation of China (Grant No. 21271022).

Institutional Review Board Statement: Not applicable.

Informed Consent Statement: Not applicable.

Data Availability Statement: New data have not been created.

Acknowledgments: We gratefully acknowledge the financial support provided by the National Natural Science Foundation of China (Grant No. 21271022).

Conflicts of Interest: The authors declare no conflict of interest.

References

1. Pareek, A.; Dom, R.; Gupta, J.; Chandran, J.; Adepu, V.; Borse, P.H. Insights into renewable hydrogen energy: Recent advances and prospects. *Mater. Sci. Energy Technol.* **2020**, *3*, 319–327. [[CrossRef](#)]
2. Wang, M.; Han, K.; Zhang, S.; Sun, L. Integration of organometallic complexes with semiconductors and other nanomaterials for photocatalytic H₂ production. *Coord. Chem. Rev.* **2015**, *287*, 1–14. [[CrossRef](#)]
3. Li, X.; Li, N.; Gao, Y.; Ge, L. Design and applications of hollow-structured nanomaterials for photocatalytic H₂ evolution and CO₂ reduction. *Chin. J. Catal.* **2022**, *43*, 679–707. [[CrossRef](#)]
4. Ahmad, H.; Kamarudin, S.K.; Minggu, L.J.; Kassim, M. Hydrogen from photo-catalytic water splitting process: A review. *Renew. Sustain. Energy Rev.* **2015**, *43*, 599–610. [[CrossRef](#)]
5. Ran, J.; Zhang, J.; Yu, J.; Jaroniec, M.; Qiao, S.Z. Earth-abundant cocatalysts for semiconductor-based photocatalytic water splitting. *Chem. Soc. Rev.* **2014**, *43*, 7787–7812. [[CrossRef](#)]
6. Wang, Y.; Ding, Z.; Arif, N.; Jiang, W.-C.; Zeng, Y.-J. 2D material based heterostructures for solar light driven photocatalytic H₂ production. *Mater. Adv.* **2022**, *3*, 3389–3417. [[CrossRef](#)]

7. Yue, M.; Lambert, H.; Pahon, E.; Roche, R.; Jemei, S.; Hissel, D. Hydrogen energy systems: A critical review of technologies, applications, trends and challenges. *Renew. Sustain. Energy Rev.* **2021**, *146*, 111180. [[CrossRef](#)]
8. Corredor, J.; Rivero, M.J.; Rangel, C.M.; Gloaguen, F.; Ortiz, I. Comprehensive review and future perspectives on the photocatalytic hydrogen production. *J. Chem. Technol. Biotechnol.* **2019**, *94*, 3049–3063. [[CrossRef](#)]
9. Bie, C.; Zhu, B.; Wang, L.; Yu, H.; Jiang, C.; Chen, T.; Yu, J. A Bifunctional CdS/MoO₂/MoS₂ Catalyst Enhances Photocatalytic H₂ Evolution and Pyruvic Acid Synthesis. *Angew. Chem. Int. Ed. Engl.* **2022**, *61*, e202212045. [[CrossRef](#)]
10. Mohite, S.V.; Kim, S.; Lee, C.; Bae, J.; Kim, Y. Z-scheme heterojunction photocatalyst: Deep eutectic solvents-assisted synthesis of Cu₂O nanocluster improved hydrogen production of TiO₂. *J. Alloys Compd.* **2022**, *928*, 167168. [[CrossRef](#)]
11. Zhang, Y.; Liu, D.; Shi, J.; Chen, P.; Zong, S.; Cheng, C.; Chen, K.; Chen, Y.; Ma, L. (Oxy)nitride heterojunction-strengthened separation of photogenerated carriers in g-C₃N₄ towards enhanced photocatalytic H₂ evolution. *Appl. Catal. A Gen.* **2022**, *643*, 118746. [[CrossRef](#)]
12. Guo, S.; Li, Y.; Xue, C.; Sun, Y.; Wu, C.; Shao, G.; Zhang, P. Controllable construction of hierarchically CdIn₂S₄/CNFs/Co₄S₃ nanofiber networks towards photocatalytic hydrogen evolution. *Chem. Eng. J.* **2021**, *419*, 129213. [[CrossRef](#)]
13. Dang, X.; Xie, M.; Dai, F.; Guo, J.; Liu, J.; Lu, X. The in situ construction of ZnIn₂S₄/CdIn₂S₄ 2D/3D nano hetero-structure for an enhanced visible-light-driven hydrogen production. *J. Mater. Chem. A* **2021**, *9*, 14888–14896. [[CrossRef](#)]
14. Zhang, H.H.; Zhan, G.P.; Liu, Z.K.; Wu, C.D. Photocatalytic Hydrogen Evolution Coupled with Production of Highly Value-Added Organic Chemicals by a Composite Photocatalyst CdIn₂S₄@MIL-53-SO₃Ni_{1/2}. *Chem. Asian J.* **2021**, *16*, 1499–1506. [[CrossRef](#)]
15. Kale, B.B.; Baeg, J.O.; Lee, S.M.; Chang, H.; Moon, S.J.; Lee, C.W. CdIn₂S₄ Nanotubes and “Marigold” Nanostructures: A Visible-Light Photocatalyst. *Adv. Funct. Mater.* **2006**, *16*, 1349–1354. [[CrossRef](#)]
16. Ma, D.; Shi, J.W.; Zou, Y.; Fan, Z.; Shi, J.; Cheng, L.; Sun, D.; Wang, Z.; Niu, C. Multiple carrier-transfer pathways in a flower-like In₂S₃/CdIn₂S₄/In₂O₃ ternary heterostructure for enhanced photocatalytic hydrogen production. *Nanoscale* **2018**, *10*, 7860–7870. [[CrossRef](#)] [[PubMed](#)]
17. Yu, Y.; Chen, G.; Wang, G.; Lv, Z. Visible-light-driven ZnIn₂S₄/CdIn₂S₄ composite photocatalyst with enhanced performance for photocatalytic H₂ evolution. *Int. J. Hydrog. Energy* **2013**, *38*, 1278–1285. [[CrossRef](#)]
18. Bai, X.; Wu, W.; Lv, H. Effects of Cu²⁺ Doping on Structure, Morphology and Photocatalytic Hydrogen Production Performance of Porous CdIn₂S₄ Microsphere. *IOP Conf. Ser. Mater. Sci. Eng.* **2020**, *735*, 012041. [[CrossRef](#)]
19. Bai, X.F.; Li, J.S. Photocatalytic Hydrogen Evolution over Cr³⁺ Doped Porous CdIn₂S₄ Photocatalysts under Visible Light Irradiation. *Adv. Mater. Res.* **2012**, *486*, 181–186. [[CrossRef](#)]
20. He, J.; Li, B.; Yu, J.; Qiao, L.; Li, S.; Zu, X.; Xiang, X. Ultra-thin CdIn₂S₄ nanosheets with nanoholes for efficient photocatalytic hydrogen evolution. *Opt. Mater.* **2020**, *108*, 110231. [[CrossRef](#)]
21. Chen, Y.; Hu, Q.; Yu, M.; Gong, X.; Li, S.; Wang, S.; Yu, H.; Li, Z. In situ construction of a direct Z-scheme CdIn₂S₄/TiO₂ heterojunction for improving photocatalytic properties. *CrystEngComm* **2021**, *23*, 5070–5077. [[CrossRef](#)]
22. Chen, X.; Li, L.; Zhang, W.; Li, Y.; Song, Q.; Dong, L. Fabricate Globular Flower-like CuS/CdIn₂S₄/ZnIn₂S₄ with High Visible Light Response via Microwave-assisted One-step Method and Its Multipathway Photoelectron Migration Properties for Hydrogen Evolution and Pollutant Degradation. *ACS Sustain. Chem. Eng.* **2016**, *4*, 6680–6688. [[CrossRef](#)]
23. Qiang, M.; Zhang, X.; Song, H.; Pi, C.; Wang, X.; Gao, B.; Zheng, Y.; Peng, X.; Chu, P.K.; Huo, K. General synthesis of nanostructured Mo₂C electrocatalysts using a carbon template for electrocatalytic applications. *Carbon* **2022**, *197*, 238–245. [[CrossRef](#)]
24. Huo, L.; Liu, B.; Zhang, G.; Zhang, J. Universal Strategy to Fabricate a Two-Dimensional Layered Mesoporous Mo₂C Electrocatalyst Hybridized on Graphene Sheets with High Activity and Durability for Hydrogen Generation. *ACS Appl. Mater. Interfaces* **2016**, *8*, 18107–18118. [[CrossRef](#)] [[PubMed](#)]
25. Ma, B.; Wang, X.; Lin, K.; Li, J.; Liu, Y.; Zhan, H.; Liu, W. A novel ultraefficient non-noble metal composite cocatalyst Mo₂N/Mo₂C/graphene for enhanced photocatalytic H₂ evolution. *Int. J. Hydrog. Energy* **2017**, *42*, 18977–18984. [[CrossRef](#)]
26. Li, H.; Hong, W.; Cui, Y.; Fan, S.; Zhu, L. Effect of Mo₂C content on the structure and photocatalytic property of Mo₂C/TiO₂ catalysts. *J. Alloys Compd.* **2013**, *569*, 45–51. [[CrossRef](#)]
27. Ma, X.; Ren, C.; Li, H.; Liu, X.; Li, X.; Han, K.; Li, W.; Zhan, Y.; Khan, A.; Chang, Z.; et al. A novel noble-metal-free Mo₂C-In₂S₃ heterojunction photocatalyst with efficient charge separation for enhanced photocatalytic H₂ evolution under visible light. *J. Colloid Interface Sci.* **2021**, *582*, 488–495. [[CrossRef](#)]
28. Yue, X.; Yi, S.; Wang, R.; Zhang, Z.; Qiu, S. Well-controlled SrTiO₃@Mo₂C core-shell nanofiber photocatalyst: Boosted photo-generated charge carriers transportation and enhanced catalytic performance for water reduction. *Nano Energy* **2018**, *47*, 463–473. [[CrossRef](#)]
29. Yue, X.; Yi, S.; Wang, R.; Zhang, Z.; Qiu, S. A novel architecture of dandelion-like Mo₂C/TiO₂ heterojunction photocatalysts towards high-performance photocatalytic hydrogen production from water splitting. *J. Mater. Chem. A* **2017**, *5*, 10591–10598. [[CrossRef](#)]
30. Zhang, J.; Wu, M.; He, B.; Wang, R.; Wang, H.; Gong, Y. Facile synthesis of rod-like g-C₃N₄ by decorating Mo₂C co-catalyst for enhanced visible-light photocatalytic activity. *Appl. Surf. Sci.* **2019**, *470*, 565–572. [[CrossRef](#)]
31. Ma, X.; Li, W.; Ren, C.; Dong, M.; Geng, L.; Fan, H.; Li, Y.; Qiu, H.; Wang, T. Construction of novel noble-metal-free MoP/CdIn₂S₄ heterojunction photocatalysts: Effective carrier separation, accelerating dynamically H₂ release and increased active sites for enhanced photocatalytic H₂ evolution. *J. Colloid Interface Sci.* **2022**, *628*, 368–377. [[CrossRef](#)] [[PubMed](#)]

32. Li, C.; Zhao, Y.; Liu, X.; Huo, P.; Yan, Y.; Wang, L.; Liao, G.; Liu, C. Interface engineering of $\text{Co}_9\text{S}_8/\text{CdIn}_2\text{S}_4$ ohmic junction for efficient photocatalytic H_2 evolution under visible light. *J. Colloid Interface Sci.* **2021**, *600*, 794–803. [[CrossRef](#)] [[PubMed](#)]
33. Sun, H.; Xue, W.; Fan, J.; Liu, E.; Yu, Q. Preparation of Ni_{12}P_5 -decorated $\text{Cd}_{0.5}\text{Zn}_{0.5}\text{S}$ for efficient photocatalytic H_2 evolution. *J. Alloys Compd.* **2021**, *854*, 156951. [[CrossRef](#)]
34. Wen, J.; Li, X.; Li, H.; Ma, S.; He, K.; Xu, Y.; Fang, Y.; Liu, W.; Gao, Q. Enhanced visible-light H_2 evolution of g- C_3N_4 photocatalysts via the synergetic effect of amorphous NiS and cheap metal-free carbon black nanoparticles as co-catalysts. *Appl. Surf. Sci.* **2015**, *358*, 204–212. [[CrossRef](#)]
35. Ma, B.; Xu, H.; Lin, K.; Li, J.; Zhan, H.; Liu, W.; Li, C. Mo_2C as Non-Noble Metal Co-Catalyst in $\text{Mo}_2\text{C}/\text{CdS}$ Composite for Enhanced Photocatalytic H_2 Evolution under Visible Light Irradiation. *ChemSusChem* **2016**, *9*, 820–824. [[CrossRef](#)]
36. Ma, X.; Li, W.; Ren, C.; Li, H.; Liu, X.; Li, X.; Wang, T.; Dong, M.; Liu, S.; Chen, S. A novel noble-metal-free binary and ternary In_2S_3 photocatalyst with WC and “W-Mo auxiliary pairs” for highly-efficient visible-light hydrogen evolution. *J. Alloys Compd.* **2021**, *875*, 160058. [[CrossRef](#)]
37. Song, Y.; Xia, K.; Gong, Y.; Chen, H.; Li, L.; Yi, J.; She, X.; Chen, Z.; Wu, J.; Li, H.; et al. Controllable synthesized heterostructure photocatalyst $\text{Mo}_2\text{C}@C/2D$ g- C_3N_4 : Enhanced catalytic performance for hydrogen production. *Dalton. Trans.* **2018**, *47*, 14706–14712. [[CrossRef](#)]
38. Xiaohui, M.; Wenjun, L.; Hongda, L.; Mei, D.; Xinyang, L.; Liang, G.; Hongxia, F.; Yanyan, L.; Hong, Q.; Tianyu, W. Fabrication of novel and noble-metal-free $\text{MoP}/\text{In}_2\text{S}_3$ Schottky heterojunction photocatalyst with efficient charge separation for enhanced photocatalytic H_2 evolution under visible light. *J. Colloid Interface Sci.* **2022**, *617*, 284–292. [[CrossRef](#)]
39. Ma, X.; Li, W.; Ren, C.; Li, H.; Li, X.; Dong, M.; Gao, Y.; Wang, T.; Zhou, H.; Li, Y. Fabrication of novel noble-metal-free $\text{ZnIn}_2\text{S}_4/\text{WC}$ Schottky junction heterojunction photocatalyst: Efficient charge separation, increased active sites and low hydrogen production overpotential for boosting visible-light H_2 evolution. *J. Alloys Compd.* **2022**, *901*, 163709. [[CrossRef](#)]
40. Ma, X.; Li, W.; Li, H.; Dong, M.; Geng, L.; Wang, T.; Zhou, H.; Li, Y.; Li, M. Novel noble-metal-free $\text{Co}_2\text{P}/\text{CdIn}_2\text{S}_4$ heterojunction photocatalysts for elevated photocatalytic H_2 production: Light absorption, charge separation and active site. *J. Colloid Interface Sci.* **2023**, *639*, 87–95. [[CrossRef](#)]
41. Zhang, B.; Shi, H.X.; Hu, X.Y.; Wang, Y.S.; Liu, E.Z.; Fan, J. A novel S-scheme $\text{MoS}_2/\text{CdIn}_2\text{S}_4$ flower-like heterojunctions with enhanced photocatalytic degradation and H_2 evolution activity. *J. Phys. D Appl. Phys.* **2020**, *53*, 205101. [[CrossRef](#)]
42. Li, Q.; Liu, W.L.; Xie, X.J.; Yang, X.L.; Chen, X.F.; Xu, X.G. Synthesis and Characterization of Amorphous Molybdenum Sulfide (MoS_x)/ CdIn_2S_4 Composite Photocatalyst: Co-Catalyst Using in the Hydrogen Evolution Reaction. *Catalysts* **2020**, *10*, 1455. [[CrossRef](#)]

Disclaimer/Publisher’s Note: The statements, opinions and data contained in all publications are solely those of the individual author(s) and contributor(s) and not of MDPI and/or the editor(s). MDPI and/or the editor(s) disclaim responsibility for any injury to people or property resulting from any ideas, methods, instructions or products referred to in the content.